PSFC/JA-02-3

An Interpretation of Fluctuation Induced Transport Derived from Electrostatic Probe Measurements

B. LaBombard

January 2002

Plasma Science and Fusion Center
Massachusetts Institute of Technology
Cambridge, MA 02139 USA

This work was supported by the U.S. Department of Energy, Cooperative Grant No. DE-FC02-99ER54512. Reproduction, translation, publication, use and disposal, in whole or in part, by or for the United States government is permitted.

Submitted for publication to *Physics of Plasmas.*

An interpretation of fluctuation induced transport derived from electrostatic probe measurements

B. LaBombard*

Massachusetts Institute of Technology, Plasma Science and Fusion Center,

175 Albany St., Cambridge, MA 02139 USA

Fluctuation-induced particle fluxes ($\Gamma_{\tilde{n}\tilde{\phi}}$) in the edge of Alcator C-Mod [Phys. Plasmas **1**, 1511 (1994)] are inferred from a fast-scanning probe using standard analysis techniques. The magnitude and profile shape of $\Gamma_{\tilde{n}\tilde{\phi}}$ is clearly inconsistent with fluxes inferred from global particle and power balance. These differences are difficult to reconcile if $\Gamma_{\tilde{n}\tilde{\phi}}$ is interpreted as a measure of the particle flux in the unperturbed plasma. However, if $\Gamma_{\tilde{n}\tilde{\phi}}$ is reinterpreted as the particle flux which must 'fill-in' the presheath zone formed by the probe, these inconsistencies are eliminated. In this case, an effective diffusivity in the presheath zone (D_{ps}) can be estimated from $\Gamma_{\tilde{n}\tilde{\phi}}$. D_{ps} is found to be in the range of diffusivities inferred from global particle balance (D_{SOL}), indirectly supporting the hypothesis. However, the profile of D_{ps} and its dependency on discharge conditions are markedly different than D_{SOL}, implying that D_{ps} is also not simply related to transport in the unperturbed plasma.

PACS: 52.25.Fi, 52.25.Gj, 52.35.Ra, 52.40.Hf, 52.55.Fa, 52.70.Ds, 52.70.Nc

---

*Tel.: 1-617-253-6942, Fax: 1-617-253-0627: e-mail: labombard@psfc.mit.edu.

I. INTRODUCTION

Electrostatic probes have clearly demonstrated their utility as a key diagnostic for characterizing local plasma conditions, both in the confinement region of low power density plasmas and in the cooler edge regions of high power density plasma fusion experiments. The ability of a probe to simultaneously record information about plasma density, electron temperature, plasma potential and fluctuations of these quantities in a spatially localized region is virtually unsurpassed by any other diagnostic. However, these measurements come at a price; one must confront potential problems in interpreting the data: Can the measured quantities be reliably related to plasma parameters in the absence of the probe? To what degree are the inferred quantities being influenced by the presence of the probe and complications associated plasma-surface interaction physics? Probe diagnosticians are usually well acquainted with such concerns. For example, corrections in electron temperature due to a non-thermal electron population and/or temperature gradients along magnetic field lines are well known[1-4]. The influence of the probe-induced presheath zone and its extent along magnetic field lines relative to nearby objects has been analyzed extensively[5-7] and measured in high density plasmas in some detail[8-10]. There is the additional constraint of power density limitations; if the electrodes become sufficiently hot then thermionic electron emission can interfere with data interpretation.

Probes are also particularly well suited for measuring plasma fluctuations. High bandwidth measurements of local floating potential and ion saturation current levels are readily made. These measurements have in turn allowed direct estimates of the fluctuation-induced fluxes in the edge plasma of many devices[11-26]. The unique utility of probes is further demonstrated as they provide a means to determine the local correlations in plasma fluctuations that give rise to other quantities such as turbulent conducted energy fluxes[27,15] and Reynolds stress[25,28], and to study in detail the intermittent events that characterize the edge plasma transport[20,21,29,30]. However, a natural question again arises: Under what conditions does the 'measurement' of cross-field turbulence-induced fluxes (and other deduced transport quantities) properly characterize the level that occurs in a

plasma *in the absence of the probe*?

Some success has been reported in relating the fluxes inferred from electrostatic probe measurements (fluctuation-induced) and fluxes inferred from global particle balance estimates. For example, pioneering measurements of particle transport in the shadow of a limiter on the Caltech Tokamak with a 2-D probe array[31] indicated that the fluctuation-induced fluxes were consistent with the fluxes into the limiter shadow cast by the probe array itself. It was reported on the Texas Experimental Tokamak (TEXT)[13,32] that the level of fluctuation-induced transport at the limiter radius was of a comparable magnitude and scaled in a similar way with discharge conditions as the particle fluxes inferred from H_α measurements and global particle balance. It was also observed that the pattern of visible light fluctuations in the edge of the plasma was unchanged when a Langmuir probe was inserted into that region[33]. These observations and others suggested that: (1) electrostatic turbulence primarily sets the level of particle transport in the edge plasma and (2) probe measurements are non-perturbing and can quantify the magnitude of the underlying turbulent transport (allowing for possible corrections from electron temperature fluctuations, which were not measured at that time).

However, when one examines the literature for fluctuation-induced flux measurements made inside closed flux surface regions or in the scrape-off layers of magnetically diverted discharges, some clear inconsistencies are evident. It is often observed that the radial-outward fluctuation-induced fluxes increase in magnitude as one moves further inside the last-closed flux surface (LCFS). This observation was first noted on the Pretext tokamak[12], was reported from experiments on TEXT[13,32], and is evident in data from the HL-1 tokamak[14] and the Advanced Toroidal Facility (ATF)[16]. Clearly, radial-outward fluxes which decrease across the plasma profile *before* the limiter shadow is encountered do not satisfy the particle continuity equation, if these fluxes are taken to be poloidally and toroidally symmetric. (Note: Volume recombination is negligible in these hot plasmas.) A notable exception to this trend is reported for the Joint European Torus (JET)[22,26]

where the radial-outward fluctuation-induced flux did indeed appear to be smaller inside the LCFS in limited and diverted discharges. There are also some special cases reported where the fluctuation-induced flux is found to be reversed, i.e., radial-inward. In the TJ-II stellarator[34], this situation was encountered and believed to be associated with the influence of a vacuum magnetic island[35]. Such observations remind us that strong poloidal asymmetries in fluctuation-induced fluxes can occur and in some cases may account for apparent inconsistencies.

It is also observed in many diverted discharges that the measured fluctuation-induced flux is much too high to be consistent with global particle balance (DIII-D tokamak[23], JET[36,22,26]). Taken together, the above observations have led to the speculation that (3) there exists some inward particle transport mechanism that does not involve fine scale plasma turbulence such as large stationary convection cells, as suggested in some experiments[37-40], and/or (4) there are large corrections that should be made to the fluctuation-induced flux estimate due to finite electron temperature fluctuations that are not being measured in many of these experiments, and/or (5) there exists a large poloidal asymmetry in the turbulent transport (ballooning hypothesis). However, with respect to speculation (4): Recent measurements in the Texas Experimental Tokamak-Upgrade (TEXT-U)[41] and in DIII-D[30] indicate that density and electron temperature fluctuations in the edge plasma tend to be in phase. Numerical turbulence simulations also result in density and electron temperature fluctuations that are in phase[42]. In this case, finite temperature fluctuation corrections would not significantly change the magnitude of the estimated particle fluxes. With respect to speculation (5): the measurements on JET[36,22,26] were made with the probe inserted from the top of the torus; it was concluded that a 'ballooning hypothesis' for turbulent transport could not by itself account for the apparent inconsistency in diverted plasmas.

One possible explanation for much of the observed particle flux inconsistencies is simply that the probe perturbs the plasma in such a way that it independently sets the magnitude of the locally inferred fluctuation-induced particle fluxes. Consider Zweben's original observation using the 2-D limiter probe array[31]: The measured fluctuation-induced fluxes were consistent with the

fluxes into the local scrape-off layer that was caused by the probe array itself. As noted above, it is well established that when a probe is inserted into a plasma it always forms a local scrape-off layer, the presheath plasma zone, where the plasma density is depressed by a factor of ~2 (in the case of a non-flowing background plasma). The disturbance scale length along the magnetic field line is set primarily by particle balance; the cross-field plasma flux into the presheath zone balances the parallel flux onto the probe body.

A simplified probe-presheath geometry is illustrated in Fig. 1. Three electrodes on the end of a probe body are used to estimate the cross-field profile of time-averaged fluctuation-induced radial particle flux density, $\Gamma_{r\tilde{n}\tilde{\phi}}(r)$. It is nearly always reported that this flux points in the $+\hat{r}$ direction, crossing into the presheath zone formed by the probe. A simple interpretation is that this turbulence-driven flux consists of two components, one which is due to the intrinsic transport of particles down the radial gradients in the plasma ($\Gamma_{r\,plasma}$) and one which is caused by the presence of the probe itself ($\Gamma_{\perp probe}$),

$$\Gamma_{r\tilde{n}\tilde{\phi}}(r) = \Gamma_{r\,plasma}(r) + \Gamma_{\perp probe}(r). \qquad (1)$$

It is expected that most of the neutrals recycling from the probe body will ionize outside the probe presheath, owing to its small cross-field extent. Therefore, in order to conserve plasma-neutral mass balance, $\Gamma_{\perp probe}$ must exist in order to supply the plasma flux which is neutralized on the probe body. Apparently, $\Gamma_{\perp probe}$ is driven by the local cross-field gradients near the edge of the probe presheath. From these considerations, it is clear that in order to interpret $\Gamma_{r\tilde{n}\tilde{\phi}}$ as an estimate of the transport fluxes in the SOL *in the absence of the probe*, one needs to be assured that $\Gamma_{\perp probe} << \Gamma_{r\tilde{n}\tilde{\phi}}$. However, if in fact there is reason to suspect that $\Gamma_{\perp probe} \sim \Gamma_{r\tilde{n}\tilde{\phi}}$, (such as was detected by Zweben's 2-D probe array [31]) then this interpretation is not justified. In this case,

$\Gamma_{r\tilde{n}\tilde{\phi}}$ is essentially the flux density needed to 'fill-in' the presheath plasma zone. An effective cross-field particle diffusion coefficient in the probe presheath can be computed from $\Gamma_{r\tilde{n}\tilde{\phi}}$, but it is not clear if this quantity relates in any direct way to the transport levels or effective cross-field particle diffusivities in the unperturbed plasma.

In this paper, measurements of fluctuation-induced particle flux profiles in ohmic heated Alcator C-Mod discharges are reported for a range in discharge densities with the aim to critically assess the reliability of an electrostatic probe to deduce the transport fluxes in the unperturbed plasma. Section II describes the plasma discharges and the experimental arrangement of the relevant diagnostics. In section III, the measured flux profiles and the cross-field heat convection profiles that they imply are compared to separate estimates of the cross-field particle and heat flux profiles. These estimates are based on global particle balance (obtained from measurements of ionization profiles and flows towards the divertor), sound speed flow towards divertor surfaces, and heat fluxes arising from parallel electron conduction in the scrape-off layer (SOL). Similar to results reported from other experiments outlined above, it is found that the fluctuation-induced particle fluxes significantly exceed the flux estimates from particle balance models. The implied heat loss from the fluctuation-induced convection also appears to be too high; it would exceed the total input power in most discharges. Also, in discharges where the probe could be inserted well inside the LCFS, the radial-outward fluctuation-induced particle flux was found to continue to increase in magnitude, in apparent contradiction to satisfying particle continuity. These observations and others suggest that the fluctuation-induced particle flux estimates made by the C-Mod probe should not be interpreted as indicative of the transport in the unperturbed plasma. Section IV considers the alternative explanation advanced above, namely, that the measured fluctuation-induced particle flux is simply the cross-field plasma flow that 'fills-in' the presheath zone formed by the probe. Two separate estimates of effective cross-field particle diffusivities in the presheath zone are made. The

magnitude of these diffusivities are found to be in the range of typical diffusivities seen in the far scrape-off layer (based on global particle balance estimates), lending some support to this new interpretation of the measurement. However, the presheath diffusivity does not appear to be directly related to the diffusivities found in the unperturbed plasma. Section V discusses the potential impact of this new interpretation on data analysis. A simple experiment is suggested to provide a more rigorous test of the hypothesis. Section VI recaps the principle findings of this work.

II. EXPERIMENT

The cross-section of a typical Alcator C-Mod discharge and diagnostics directly relevant to the present experiments is shown in Fig.2. Results reported in this paper were obtained from ohmic heated deuterium discharges with plasma currents (I_p) between 0.76 and 0.80 MA, toroidal magnetic field (B_T) of 5.3 tesla, and line-averaged plasma densities spanning the range, $1.0 < \bar{n}_e < 3.0 \times 10^{20}$ m^{-3} . In all cases, the plasma had a lower single-null magnetic equilibrium, similar to that shown in Fig. 2. Further information on Alcator C-Mod's design, diagnostics, and operational characteristics can be found in Ref.[43]

Two scanning probe systems are used to sample plasma in main-chamber scrape-off layer up to and sometimes inside the separatrix (see Fig.2): a vertical-scanning probe located at a position 'upstream' from the entrance to the outer divertor, and a horizontal-scanning probe that records plasma conditions 10 cm above the outer midplane. Both probes can be scanned up to three times in a single discharge to traverse into and out of the scrape-off layer plasma with a peak velocity of ~1 m s^{-1}.

The primary focus of this paper is on data collected by the horizontal scanning probe. The geometry of this probe is shown in fig. 3. Facets are cut into the plasma-facing end of a 19 mm diameter molybdenum probe body to form a pyramidal surface. Four 1.5 mm diameter tungsten electrodes penetrate the pyramid through holes at locations equidistant from the peak of the

pyramid and coincident with the four edges of the pyramid. The tungsten wires are insulated with ceramic coatings (0.18 mm thick) and cut so that their ends are flush to the pyramidal surface. This geometry is found to work well in C-Mod's high power density plasmas since it presents a large surface area to heat flux flowing along magnetic field lines. The edges of the pyramid are oriented such that a magnetic field line which enters through the center of the WEST electrode proceeds through the pyramid and exits through the center of the EAST electrode. Thus the EAST and WEST electrodes sample plasma from opposite directions along the same field line. In contrast, the NORTH and SOUTH electrodes sample plasma from both directions on their respective magnetic field lines. The grazing angle between magnetic field lines and the pyramidal surfaces is approximately 20 degrees and the pyramid is oriented so that all four electrodes lie on the same magnetic flux surface. The vertical probe has a similar geometry except that the spacing between tungsten wires is a factor of two larger, the probe body is 16 mm in diameter, and a orifice is located at the center of the pyramid to enable the injection of gaseous impurities[44].

For the data presented in this paper, the NORTH and SOUTH electrodes on the horizontal scanning probe where operated in a floating-voltage mode and the EAST and WEST electrodes were operated in a swept-voltage mode (2 kHz sweep, -300 to 100 volts maximum bias range with a 2 amp current clamp). Time instantaneous voltage and current data from all electrodes were sampled at 1MHz. By fitting positive and negative-going *I-V* characteristics, densities and temperatures along each probe's trajectory are obtained every 0.25 ms (corresponding to ~0.25 mm of probe travel). Time series data of ion saturation currents (EAST and WEST electrodes) and floating potentials (NORTH and SOUTH electrodes) were extracted from the horizontal probe data stream during time periods when the EAST and WEST electrodes demonstrated to be saturated ion collection. Typical durations of the time segments were ~120 μs. These time series segments were found to yield similar fluctuation power spectra and time-averaged fluctuation-induced fluxes (although with higher statistical noise) as very long time segments (~ 200 ms), obtained when the

EAST and WEST electrodes where continuously biased in ion saturation and held at a fixed spatial location[21].

The EAST and WEST electrodes can also function as a 'Mach probe' pair in which plasma flow along the local magnetic field can be estimated from the ratio of ion saturation currents[6]. As a result, density, temperature, floating potential, and parallel flow measurements from the vertical scanning probe can be used to estimate cross-field profiles of both parallel and *ExB* flows. By integrating the poloidal projection of these flows along the trajectory of the vertical scanning probe, the total particle flux directed towards the lower divertor structure can be estimated. These measurements, combined with midplane Ly_α brightnesses[45], are used to estimate cross-field particle flux profiles in Alcator C-Mod. Figure 2 shows the locations of the toroidally-viewing Ly_α chords. Details of the analysis technique can be found in Ref.[46]

Cross-field profiles of density, electron temperature, Ly_α emissivity, and local ionization rate for the set of discharges under study here are shown in Fig. 4. The density and temperature profiles are smooth spline fits to raw data obtained from the horizontal scanning probe. The Ly_α emissivity profiles are obtained from an Abel inversion of the Ly_α brightness profiles. The local ionization profiles are computed from the local Ly_α emissivity and the measured density and temperature profiles using Johnson-Hinnov rate coefficients[47]. Note that at these electron temperatures, volume recombination is negligible. All data are plotted versus the distance outside the last closed flux surface at the outer midplane, ρ. It should be noted that in order to get a match between the electron pressure profiles measured by scanning probes, divertor probes (data not shown), and edge Thomson scattering system (data not shown), their relative flux surface mappings in ρ must be adjusted by a few mm. These adjustments are systematically made here to 'align' the data from these diagnostics with an estimated accuracy of ~2 mm. In any case, the principal results presented in this paper are not sensitive to these mapping corrections; any 'adjustment' that is made

to the horizontal scanning probe data is also applied to the Ly_α emissivity data and subsequently to the ionization rate profile.

The data in Fig. 4 correspond to 13 different 'scans' of the horizontal probe. All discharges had I_p between 0.76 and 0.80 MA and B_T of 5.3 tesla. The data fall into 5 groups corresponding to the line-averaged densities that were programmed: $\bar{n}_e \approx$ 1.0, 1.5, 1.8, 2.4, and 3.0 $\times 10^{20}$ m^{-3}. Notice that as $\bar{n}_e$ is increased to the highest values, the electron temperature near the separatrix drops. This behavior has been studied in some detail and appears to be related to an increase in the convected power losses across the scrape-off layer as $\bar{n}_e$ approaches about 1/2 the Greenwald density[48]. For the cases when $\bar{n}_e \approx 3.0 \times 10^{20}$ m^{-3}, the electron temperature near the separatrix is low enough to allow the horizontal scanning probe to penetrate almost 10 mm inside the separatrix without overheating. The Ly_α emissivity profiles and the derived ionization source profiles show an expected behavior as the plasma density is raised: Ionization in the scrape-off layer and inside the separatrix increases with discharge density. In all cases, the ionization rate increases with distance across the separatrix into the SOL and decreases with distance across the separatrix into the core plasma.

III. FLUCTUATION-INDUCED FLUXES

A. Computation

From the four electrodes on the horizontal scanning probe, the fluctuation-induced cross-field particle flux can be estimated. The local floating potential (V), plasma potential (ϕ), and electron temperature (T_e) are expected to be related by sheath physics,

$$\phi = V + \alpha T_e \,, \qquad (2)$$

with the coefficient α having the value of 2.8 for a deuterium plasma [49]. The ion saturation current

(I) is related to the density (n), the probe area projected along the magnetic field line (A), and the electron temperature (assuming $T_i \approx T_e$) by

$$I \approx 0.5 A n \sqrt{\frac{2\kappa T_e}{m_i}}. \qquad (3)$$

(Note: The coefficient, 0.5, can vary depending on the ratio of cross-field momentum to particle diffusivities[6]. When this ratio is 1, the coefficient can become ~0.3. However, the value of 0.5 is consistently used in this paper.) If one assumes that corrections arising from finite electron temperature fluctuations can be ignored then the NORTH and SOUTH electrodes directly record information about poloidal electric field fluctuations while the EAST and WEST electrodes record information about density fluctuations. The time-averaged radial-outward flux arising from the local turbulence can be estimated directly from the current and voltage time series data,

$$\Gamma_{r\tilde{n}\tilde{\phi}} = \frac{\langle n \rangle \left\langle \left(\tilde{I}_{East} + \tilde{I}_{West} \right) \left(\tilde{V}_{South} - \tilde{V}_{North} \right) \right\rangle}{\left\langle \tilde{I}_{East} + \tilde{I}_{West} \right\rangle d\, B} \approx \left\langle \tilde{n} \tilde{v}_r \right\rangle, \qquad (4)$$

making use of the symmetry in the probe geometry. Here, $\langle n \rangle$ is the time-averaged plasma density obtained from the usual fit of the I-V characteristic (results shown in Fig. 4), d is the cross-field spacing between the NORTH and SOUTH electrodes, B is the local magnetic field strength and the quantities $\tilde{I}$ and $\tilde{V}$ correspond to the time series data with mean values subtracted. Alternatively, the time series data can be Fourier analyzed and the flux can be computed from real part of the cross-power between density and electric field fluctuations,

$$\Gamma_{r\tilde{n}\tilde{\phi}} = c \int \mathrm{Re}\{n_\omega\, ik_\theta\, \phi_\omega^*\}) \delta\omega / B \approx \left\langle \tilde{n} \tilde{v}_r \right\rangle, \qquad (5)$$

making use of frequency-resolved poloidal wavenumber of the potential fluctuations (k_θ), estimated from a two-point correlation method[50]. When electron temperature fluctuations can be safely ignored, $c = 1$. However, recent measurements [30,41] and numerical simulation[42] suggest that

temperature fluctuations in the edge plasma are at the level $\tilde{T}_e / T_e \approx \tilde{n} / n$ with temperature and density fluctuations in phase. In this case, a correction to the flux estimate from finite $\tilde{T}_e$ in Eq. (3) contributes, resulting in $c \approx 1/(1+0.5\tilde{T}_e / T_e)$. Thus the magnitude of $\Gamma_{r\tilde{n}\tilde{\phi}}$ could be justifiably reduced from that suggested by Eq. (4), but by only about ~30% at most. In this paper, no finite $\tilde{T}_e$ corrections are made; Eq. (5) is used with $c = 1$. (Computation of $\Gamma_{r\tilde{n}\tilde{\phi}}$ via Eq. (4) yields identical results.)

B. Fluctuation-induced particle and heat flux profiles

Cross-field profiles of fluctuation-induced particle flux density ($\Gamma_{r\tilde{n}\tilde{\phi}}$) and convected energy flux density ($5T_e\,\Gamma_{r\tilde{n}\tilde{\phi}}$, assuming $T_i \approx T_e$) computed from horizontal scanning probe data are shown in Fig. 5 for the same set of discharges shown in Fig. 4. Each symbol corresponds to a separate computation of $\Gamma_{r\tilde{n}\tilde{\phi}}$ involving the average of three or more time-series realizations of about ~120 μs length. Note that in addition to heat convection, radial-outward turbulent heat transport is also expected from triple correlations between $\tilde{T}_e$, $\tilde{n}$, and $\tilde{E}_\theta$, which is not included here. The main-chamber limiter was maintained at a location of $\rho \geq 15$ mm in these discharges.

A number of important observations can be drawn from the profiles shown in Fig.5:

(1) The cross-field fluxes are positive everywhere, suggesting a flow of particles and associated heat convection directed radial-outward everywhere.

(2) $\Gamma_{r\tilde{n}\tilde{\phi}}$ is either nearly flat (e.g., lowest density case) or is a decreasing function of ρ. At high densities, $\Gamma_{r\tilde{n}\tilde{\phi}}$ drops by a factor of ~4 across the profile with $\rho > 0$.

(3) For the highest density discharges in which the probe could be inserted well inside of

the separatrix, $\Gamma_{r\tilde{n}\tilde{\phi}}$ is found to continue to increase with distance inside the separatrix, exceeding the separatrix values by a factor of ~3 at ρ ~-10 mm.

(4) The magnitude of $\Gamma_{r\tilde{n}\tilde{\phi}}$ generally increases by a factor of almost ~8 as the density is increased from low to moderate densities ($1.0 \leq \bar{n}_e \leq 2.4 \times 10^{20}$ m^{-3})

(5) But, $\Gamma_{r\tilde{n}\tilde{\phi}}$ does not continue to increase (actually decreases) as the highest density is approached.

(6) The inferred cross-field heat convection profile shows similar trends with an augmented spatial variation owing to the electron temperature profile. For the highest density discharge, the cross-field heat convection is seen to drop by a dramatic factor of ~10 in going from ~10 mm inside the separatrix to the separatrix location.

Some of these observations appear as a serious challenge to the idea that $\Gamma_{r\tilde{n}\tilde{\phi}}$ is a measure of the transport fluxes in the unperturbed plasma. Observations (1) and (2) are not inconsistent with the expected behavior of cross-field fluxes in the unperturbed SOL plasma; one might expect that the reduction in $\Gamma_{r\tilde{n}\tilde{\phi}}$ across the SOL is just balanced by plasma flow along field lines towards the divertor. However, observation (3) [and perhaps (6)] point to a potentially severe inconsistency: How can the particle flux decrease across the profile in a region of closed magnetic field lines where recombination is negligible? As pointed out in the introduction, this phenomenon has been seen before in a number of other experiments. Observation (4) appears consistent with the increased ionization level (see Fig. 3) that is needed inside the separatrix to achieve the higher density plasmas. But observation (5) is a puzzle in this regard; it is difficult to explain how a higher density discharge appears to involve a lower particle flux through its boundary. (These are all L-mode confinement discharges.) In order to reconcile observations (3) and (5), one might be tempted to postulate the existence of a complicated 3-D flow pattern that sets in for the highest density

discharges: strong parallel flows, inward radial pinches, and preferential loss of plasma across the separatrix at a poloidal location other than at the midplane. However, there is no way at present to investigate such a contrived set of circumstances on Alcator C-Mod.

Another important test is to quantitatively compare $\Gamma_{r\tilde{n}\tilde{\phi}}$ and $5T_e\Gamma_{r\tilde{n}\tilde{\phi}}$ with fluxes derived independently from global particle and energy balance. Such comparisons are made in the following two subsections.

C. Comparison with global particle balance

Two models are used to estimate and to bound the magnitude of cross-field fluxes from global particle balance constraints.

1. SOL particle continuity model

The details of this model and its benchmark against 2-D transport code results is described in Refs. [46,48]. The model attempts to derive a cross-field particle flux profile in the SOL based on a solution to the plasma continuity equation, that accounts for the observed Ly_α brightness profiles (ionization rates), the total plasma flow directed towards the divertor (inferred from the vertical scanning probe), and the flux of plasma arriving on a main-chamber limiter. The particle fluxes inferred from this model support a conclusion that a large fraction of the plasma flux crossing the SOL in Alcator C-Mod arrives on main-chamber wall surfaces rather than flows towards divertor surfaces. For the discharges analyzed here, the ratio of total plasma flow to the divertor divided by particle flow to the wall is taken to be 0.5, which is found to be consistent with experimental measurements and 2-D transport modeling[46,48]. A key output of the model is the cross-field profile of $A_{sep}\Gamma_{PC}$ (s^{-1}) for a given discharge, which is the area of the last closed flux surface times the cross field particle flux density. In the following figures and text, this model will be referred to as the 'particle continuity model'.

2. Mach 1 flow model

In this model, any experimental information about flows and ionization in the SOL is treated with suspicion and ignored. The SOL plasma is simply assumed to be completely exhausted by flows towards the divertor with velocity equal to the sound speed at a vertical location in the poloidal cross-section corresponding to the height of the lower X-point. It is assumed that no ionization occurs in the SOL above the X-point height. Integrating the source-free continuity equation across the profile leads to an expression for $A_{sep}\Gamma_{M1}$,

$$A_{sep}\Gamma_{M1} = A_{sep}\int_{\rho}^{\rho_{\max}} \frac{n}{L_{//}}\sqrt{\frac{2\kappa T_e}{m_i}}\,\partial\rho', \qquad (6)$$

which is an estimate of the total particle flux crossing a flux surface in the SOL. Here $L_{//}$ is the distance along field lines in the SOL from inner X-point height to outer X-point height. (The value of $L_{//}$ at the separatrix is taken to be the same as at the location 1 mm into the SOL.) The measured density and temperature profiles from Fig. 3 are used in the integrand and the upper limit corresponds to the location of the last data point in the far SOL. Thus a boundary condition of zero cross-field flux to main-chamber limiter surfaces is imposed. The particle flux crossing the separatrix from Eq. (6) may be considered as an upper bound estimate of the true flux; all ionization is forced to occur inside the separatrix. Also for this reason, Eq. (6) computes the strongest possible decrease in the cross-field particle flux with radius; any ionization in the SOL would tend to flatten the flux profile. In the following figures and text, this model will be referred to as the 'Mach 1 flow model'.

3. Particle flux comparison

Figure 6 shows a comparison of the measured flux profiles of $A_{sep}\,\Gamma_{r\tilde{n}\tilde{\phi}}$, and particle flux profiles, $A_{sep}\,\Gamma_{PC}$ and $A_{sep}\Gamma_{M1}$, computed from the particle continuity and Mach 1 flow models

described above. The cross-field profiles are for three discharge densities ($\bar{n}_e$ = 1.0, 1.8 and 3.0 x10^{20} m^{-3}), corresponding to the data shown in Figs. 4 and 5. Some important observations can be made based on Fig. 6:

(1) The magnitude of $A_{sep}\,\Gamma_{r\tilde{n}\tilde{\phi}}$ is clearly inconsistent with particle balance, being systematically high. At the separatrix, $A_{sep}\,\Gamma_{r\tilde{n}\tilde{\phi}}$ can exceed the particle continuity model by a factor of ~10 and the Mach flow model by a factor of ~3.

(2) As pointed out in section III.B, the shapes of the $A_{sep}\,\Gamma_{r\tilde{n}\tilde{\phi}}$ profiles inside the separatrix (high density discharge) are also inconsistent with particle balance considerations; $A_{sep}\,\Gamma_{r\tilde{n}\tilde{\phi}}$ is found to decrease as the separatrix is approached while ionization in the particle continuity model causes $A_{sep}\,\Gamma_{PC}$ to increase as the separatrix is approached. The quantitative discrepancy in these fluxes exceeds a factor of 10 for locations inside the separatrix.

(3) Although the magnitude is too high, the shape of the $A_{sep}\,\Gamma_{r\tilde{n}\tilde{\phi}}$ profile appears to match the Mach 1 flow model better than the particle continuity model.

Accepting that $\Gamma_{r\tilde{n}\tilde{\phi}}$ is a measure of the particle fluxes in the unperturbed plasma, these quantitative discrepancies are hard to reconcile. Ballooning-like transport and/or inaccuracies in the particle balance model might explain observation (1) but would fail to explain observation (2). However, observation (3) hints at a potential explanation; it suggests that a component of $A_{sep}\,\Gamma_{r\tilde{n}\tilde{\phi}}$ may be proportional to sound speed fluxes in the SOL. This observation sparks the idea that the cross-field fluxes measured by the probe are due to plasma flow onto the probe itself. In

this case, the apparent discrepancy from observation (2) could be resolved: $A_{sep}\,\Gamma_{r\tilde{n}\tilde{\phi}}$ continues to increase with distance inside the separatrix simply because the plasma flux onto the probe continues to increase with distance inside the separatrix.

D. Comparison with global power balance constraints

The estimate of cross-field convected power carried by fluctuation-induced fluxes ($5T_e\,A_{sep}\,\Gamma_{r\tilde{n}\tilde{\phi}}$) can be compared to three independently derived quantities related to global power balance: (a) the total power crossing into the SOL (P_{sol}) derived from ohmic input power (P_{OH}) minus radiation (P_{rad}), (b) the convected power associated with the particle flux from the particle continuity model ($5T_e\,A_{sep}\,\Gamma_{PC}$), and (c) an estimate of the power that must flow across the SOL to support the electron heat conduction along open field lines to the divertor (Q_{div}). The computation of the first two quantities is straightforward. The method used to estimate Q_{div} is now described.

1. Estimate of Q_{div}

The parallel heat flux arising from electron conduction is $q_{//} = -\frac{2}{7}\kappa_0 \nabla_{//} T_e^{7/2}$ with $\kappa_0 \approx$ $2.8\text{x}10^3$ in units of watts m^{-1} $\text{eV}^{-7/2}$. Assuming a T_e profile along a field line that is symmetric with respect to the divertor targets, an equivalent uniform volumetric heat loss along the length of the field line can be constructed, $S = \nabla_{//} \cdot q_{//} \approx \frac{4}{7\pi^2 R^2 q^2}\kappa_0 (T_0^{7/2} - T_w^{7/2})$, where q is the safety factor (evaluated at 95% flux surface), R is major radius, T_0 is the peak electron temperature on the field line ($\approx T_e$ measured by horizontal probe) and T_W is the temperature at the divertor surface. An estimate of the cross-field power necessary to support electron parallel conduction losses in the

SOL beyond the flux surface at location ρ can therefore be obtained by integrating S over the volume between that flux surface and the one next to main-chamber limiter surfaces,

$$Q_{div}(\rho) \approx A_{sep}\,\frac{4}{7}\,\frac{\kappa_0}{\pi^2 R^2 q^2}\int_{\rho}^{\rho_{\max}} T_0^{\,7/2}\,\partial\rho' \,. \qquad (7)$$

For most of the range in ρ, the integral is insensitive to the assumed value of $\rho_{\max}$ since the integrand decreases rapidly with ρ. Equation (7) may be considered an upper estimate of Q_{div} since it sets T_W to zero.

2. Power flux comparison

Figure 7 shows a comparison of the convected power flux, $5T_e A_{sep}\Gamma_{r\tilde{n}\tilde{\phi}}$, with the power fluxes estimated from $5T_e A_{sep}\Gamma_{PC}$ and Q_{div}. Cross-field profiles are computed for three discharge densities ($\bar{n}_e$ = 1.0, 1.8 and 3.0 x10^{20} m^{-3}), corresponding to that in Fig. 6. In addition, the level of total input power (P_{OH}) and power into the SOL (P_{sol}) is indicated. Some important observations can be drawn from the comparisons in Fig. 7:

(1) Consistent with the observations made from the particle flux comparisons, the heat fluxes carried by $5T_e A_{sep}\Gamma_{r\tilde{n}\tilde{\phi}}$ appear too high. In the moderate and high density discharges, this component of the power crossing the separatrix (turbulent conduction is not included here) already exceeds P_{sol}, and even P_{OH} in the moderate density case.

(2) Again there appears to be a problem with the magnitude and shape of $\Gamma_{r\tilde{n}\tilde{\phi}}$ inside the separatrix: $5T_e A_{sep}\Gamma_{r\tilde{n}\tilde{\phi}}$ continues to rise to large values inside the separatrix, exceeding the input power of the discharge by a factor of ~3 or more.

(3) In all discharges it is found that $5T_e A_{sep}\Gamma_{r\tilde{n}\tilde{\phi}}$ exceeds Q_{div} by a factor of 2 to 10

across the SOL, yet the magnitude of $5T_e A_{sep} \Gamma_{r\tilde{n}\tilde{\phi}}$ decreases with distance into the SOL.

Observations (1) and (2) are just manifestations of the problems already identified in the particle flux comparison, but independently confirmed here by power balance considerations. Observation (3) presents another puzzle: If the magnitude of $5T_e A_{sep} \Gamma_{r\tilde{n}\tilde{\phi}}$ is approximately correct (as it might be argued for the low density case), what is the mechanism that causes $5T_e A_{sep} \Gamma_{r\tilde{n}\tilde{\phi}}$ to reduce by a factor of 10 in going from ρ = 0 to 15 mm? Heat loss by parallel condition to the divertor is quantitatively insufficient to account for this reduction. One explanation could be that most of the power into the SOL is radiated and does not conduct to the divertor or convect to the main-chamber walls. However, no significant radiation in the SOL is detected; such radiation would be included in the measurement of P_{rad} and this quantity is especially small in the low density case.

IV. CROSS-FIELD FLUXES INTO PROBE PRESHEATH

An ideal probe design for detecting the fluctuation-induced flux in the unperturbed plasma ($\Gamma_{r\,plasma}$) would be one which to exposes only the active areas of the electrodes to the plasma (Fig. 8a). In this way, the perturbation to the ambient plasma fluxes would be minimized and one might be confident that $\Gamma_{r\,plasma} \approx \Gamma_{r\tilde{n}\tilde{\phi}}$. However, this arrangement is not physically possible; there must be some kind of 'probe body' to provided mechanical support and means for electrical connections.

Consider a case when the projection of the probe body along field lines can be represented as a disk with radius a. Here, a is taken to be small compared to the cross-field scale lengths of the time-averaged plasma conditions (Fig. 8b). Owing to the presence of the probe body, there will

be a radial flux passing by the electrodes ($\Gamma_{\perp probe}$), attempting to 'fill-in' the presheath and maintaining the plasma flow along field lines to the probe body. If electrostatic turbulence is the dominant cross-field transport mechanism in the plasma, then the sum of both fluxes will be detected by the electrodes ($\Gamma_{r\tilde{n}\tilde{\phi}}$). The actual probe geometry (Fig. 8c) leads to the same behavior with additional complexities: The vertical height of the probe shadow ($2a$) can be larger than the gradient scale lengths of the background plasma and $\Gamma_{\perp probe}$ varies along the horizontal extent. In either case, $\Gamma_{r\tilde{n}\tilde{\phi}}$ may be interpreted as a reliable estimate of $\Gamma_{r\,plasma}$ only if $\Gamma_{\perp probe}$ in the vicinity of the electrodes is much smaller than the measured value, $\Gamma_{r\tilde{n}\tilde{\phi}}$.

The strategy used in this section of the paper is to assume that $\Gamma_{\perp probe}$ is in fact much larger than $\Gamma_{r\,plasma}$ such that the measurement, $\Gamma_{r\tilde{n}\tilde{\phi}}$, is essentially a direct measurement of $\Gamma_{\perp probe}$. This allows a characteristic length of the presheath (L') or equivalently a characteristic diffusion coefficient in the presheath ($D'_{\perp ps}$) to be estimated from local particle balance. Two local particle balance models are considered in the following subsections: a probe disk model (Fig. 8b) and a model that attempts to correct for probe geometry and plasma profile effects (Fig. 8c). Given separate estimates of the *actual* presheath values (L or $D_{\perp ps}$), one could in principle test if the hypothesis is valid: If L' is comparable to L, or $D'_{\perp ps}$ is comparable to $D_{\perp ps}$ then indeed the assumption $\Gamma_{\perp probe} << \Gamma_{r\tilde{n}\tilde{\phi}}$ is not justified; the flux densities would be of the same order.

At present, there is no independent measurement of L or $D_{\perp ps}$ available in C-Mod. Instead, values of $D'_{\perp ps}$ are compared to *unperturbed* cross-field diffusivities estimated from the SOL particle continuity model ($D_{\perp SOL}$). It is found that $D'_{\perp ps}$ lies in the range of typical $D_{\perp SOL}$

values. This indirectly supports the hypothesis that $\Gamma_{r\tilde{n}\tilde{\phi}} \sim \Gamma_{\perp probe}$. It also suggests that $\Gamma_{r\tilde{n}\tilde{\phi}}$ could be reinterpreted as a direct measurement of $D_{\perp ps}$. However, as discussed below, the profiles of $D'_{\perp ps}$ and $D_{\perp SOL}$ are sufficiently different to keep one from concluding that the $\Gamma_{r\tilde{n}\tilde{\phi}}$ can be reinterpreted as a direct measure of $D_{\perp SOL}$.

A. Ionization in the presheath zone

In the analysis to follow it is assumed that most of the neutrals that recycle from the probe body ionize outside of the probe's presheath region. This allows the flux crossing into the presheath zone to be equated to the flux arriving on the probe body. A crude estimate of the validity of this assumption can be made. It is well established that incident ions recycle from a material surface primarily as promptly reflected atoms (with probability of ~0.5 and reflected energy of ~30 eV for a 100 eV deuteron on a molybdenum surface) and molecules [51]. The molecules promptly dissociate with resultant atom energies of ~3 eV. The rate of local electron impact ionization is $\leq 3 \times 10^{-14}$ $m^{-3}s^{-1}$ for the plasma conditions shown in Fig. 4 [52]. This yields ionization mean free paths (MFP) of $\geq$ ~18 mm and $\geq$ ~6 mm respectively for the resultant fast and slow atoms in a plasma with density ~10^{20} m^{-3}. The fast atoms tend to leave the surface with a cosine distribution, aligned with the surface normal. The molecular breakup leads to an isotropic distribution of slow atoms. Owing to the inclined surfaces on the probe body (see Fig. 3), most of the neutral reflux near the end of the probe (a region of highest density, lowest MFP) is directed towards the unperturbed plasma across a narrow presheath zone. Therefore for the probe body shown in Fig. 3 ($a \sim 9.5$ mm), it is a reasonable first approximation to assume that ionization in the presheath zone can be neglected. At the highest densities, one might expect the fraction of neutral reflux ionized in the presheath to be around ~0.3.

B. Probe disk model

The properties of the magnetized presheath plasma formed by a disk probe has been studied in some detail in connection with the development of Mach probe theories[53,54,6,7]. The models assume a characteristic cross-field particle diffusivity, $D_{\perp ps}$, and the influence of cross-field momentum transport from finite viscosity has been investigated. Hutchinson[6] computed 2-D density and parallel flow velocity profiles for the case of zero background plasma flow and a ratio of particle to parallel momentum diffusivity equal to unity. The 2-D numerical simulation showed that the length of the density perturbation extends along field lines over a distance, L, and quantitatively corresponds to the expected scaling relationship,

$$L \approx \frac{a^2 C_s}{2 D_{\perp ps}}, \tag{8}$$

where C_s is the plasma sound speed. Consequently, the cross-field flux into the presheath zone also decreases with this characteristic decay length along the field line. As long as the presheath of the probe is 'free-standing', i.e., L does not extend into the presheath zone of other material surfaces, the ion saturation flux density averaged over the area of the probe projected along magnetic field lines is close to the familiar value, $J_{sat} \approx 0.5 n C_s$, independent of the size of the probe. Here n is the ambient density in the surrounding plasma.

Equating the cross-field flux to the plasma collection on the probe surface leads to the relationships,

$$\Gamma_{\perp probe} \approx \frac{a J_{sat}}{2L} \approx \frac{D_{\perp ps} n}{2a} \quad , \tag{9}$$

where $\Gamma_{\perp probe}$ is the magnitude of the cross-field flux near the electrodes caused by the presence of the probe body. Therefore, this model leads to the expressions,

$$L' \approx \frac{a\, J_{sat}}{2\Gamma_{r\tilde{n}\tilde{\phi}}} \quad ; \quad D'_{\perp ps} \approx \frac{2\, a\, \Gamma_{r\tilde{n}\tilde{\phi}}}{n} \quad . \tag{10}$$

C. Geometry and profile corrected model

Consider the particle flux crossing into the shadow of the probe body in Fig. 8c. It may be assumed that at a given radial location in the plasma (r), the cross-field flux densities directed radially and poloidally across the boundaries of the probe shadow near the probe body proceed at the same rate, $\Gamma_{\perp probe}(r)$, and that this rate is equal to the value measured by the electrostatic probes, $\Gamma_{r\tilde{n}\tilde{\phi}}(r)$. In general, the characteristic length of the presheath zone can also be a function of radius, $L(r)$. Based on this model, the total flux of particles into the volume of the probe shadow can be estimated as

$$I_{shadow} \approx 2aL'\Gamma_{r\tilde{n}\tilde{\phi}} + 2\int_{r}^{b} L'\Gamma_{r\tilde{n}\tilde{\phi}}\partial r'. \tag{11}$$

As a practical matter, the upper limit to the integral must be set to a finite value, b, corresponding to the location where some other objects in the plasma (local limiters or wall) begin to shadow the probe along field lines. Therefore, equation (11) is a valid approximation only for those values of r where it can be demonstrated that I_{shadow} is insensitive to the choice for b.

The ion saturation flux density profile along the surface of the probe body, J_{sat}, can be assumed to be similar to that quantity measured by the electrodes on the end of the probe body as the probe is scanned across the SOL . The total plasma flux arriving on one side of the probe body can therefore be estimated from,

$$I_{body} \approx 2a\int_{r}^{b} J_{sat}\partial r'. \tag{12}$$

Again, this is a valid approximation for only those values of r where I_{body} is insensitive to the choice for b.

If neutrals recycling from the probe body ionize primarily outside the presheath zone, then particle balance requires, $I_{body} \approx I_{shadow}$. From Eqs. (11) and (12), the characteristic length of the probe shadow must satisfy

$$L'\Gamma_{r\tilde{n}\tilde{\phi}} + \frac{1}{a}\int_r^b L'\Gamma_{r\tilde{n}\tilde{\phi}}\partial r' \approx \int_r^b J_{sat}\partial r'. \tag{13}$$

This relationship can also be written in a differential form,

$$\frac{\partial}{\partial r}\left(L'\Gamma_{r\tilde{n}\tilde{\phi}}\right) - \frac{1}{a}L'\Gamma_{r\tilde{n}\tilde{\phi}} = -J_{sat}, \tag{14}$$

or equivalently,

$$\frac{\partial}{\partial r}\left(L'\Gamma_{r\tilde{n}\tilde{\phi}}e^{-r/a}\right) = -J_{sat}e^{-r/a} \quad . \tag{15}$$

Integrating Eq. (15) yields

$$L'\Gamma_{r\tilde{n}\tilde{\phi}} = \int_r^b J_{sat}e^{-(r'-r)/a}\partial r' + L'(b)\Gamma_{r\tilde{n}\tilde{\phi}}(b)e^{-(b-r)/a}. \tag{16}$$

Again, Eq. (16) is a valid estimate of $L'(r)$ only for those values of r where $L'\Gamma_{r\tilde{n}\tilde{\phi}}$ is insensitive to the choice for b and to the value of $L'(b)$. Therefore, for this restricted range of r, Eq. (16) becomes

$$L' \approx \frac{1}{\Gamma_{r\tilde{n}\tilde{\phi}}}\int_r^b J_{sat}e^{-(r'-r)/a}\partial r', \qquad (r < r_{\max}). \tag{17}$$

Comparing this expression with Eq. (10), one can see that the effect of the geometry and profile corrections is to replace the scale length, a, in the probe disk model with a hybrid scale length, involving a and the radial decay length of J_{sat}. As might be expected, these expressions become

identical when J_{sat} decays with an e-folding length of a. Therefore from Eq. (8),

$$D'_{\perp ps}(r) \approx \frac{4\Gamma_{r\tilde{n}\tilde{\phi}} \int_{r}^{b} J_{sat} e^{-(r'-r)/a} \partial r'}{n J_{sat}}, \qquad (r < r_{\max}). \qquad (18)$$

D. Comparison of $D'_{\perp ps}$ and $D_{\perp SOL}$

Figure 9 shows a comparison of $D'_{\perp ps}$ profiles inferred from Eqs. (10) and (18) and $D_{\perp SOL}$ profiles estimated from the SOL particle continuity model (outlined in section III.C.1). $D_{\perp SOL}$ is the effective cross-field particle diffusivity in the unperturbed SOL derived from flux and gradient measurements, $D_{\perp SOL} \equiv -\Gamma_{PC} / \nabla n$. (Note that this is simply a definition. Experimental evidence suggests that a local diffusion description of transport in the far SOL may not be appropriate; cross-field fluxes occur in the far SOL in Alcator C-Mod even when the density profile is flat[55,56,46,48]. This result is evident in Fig. (9): $D_{\perp SOL}$ tends to 'blow up' in a region near ρ ~10 mm, owing to the nearly flat density profile there in high density discharges.)

Some observations can be made based on the comparison in Fig. 9:

(1) Both local particle balance models yield comparable $D'_{\perp ps}$ values with a strong variation in $D'_{\perp ps}$ across the profile (particularity from the 'geometry and profile corrected' model), depending on discharge density: The lowest density discharge shows nearly a factor of 10 drop in $D'_{\perp ps}$ near the separatrix while the highest density discharge shows no such variation.

(2) Values of $D'_{\perp ps}$ are remarkably insensitive to the discharge density for $\rho >$ 5 mm. Typical values are $D'_{\perp ps} \sim 1$ m^{-2} s^{-1}.

(3) $D_{\perp SOL}$ also shows a strong variation across the profile (factor of 10), but the variation persists independent of discharge density; the entire profile increases with discharge density.

(4) Values for $D_{\perp SOL}$ in the region ρ > 5 mm range between 0.1 and 10.0.

From observations (2) and (4), it appears possible that $D'_{\perp ps}$ represents the true magnitude of cross-field diffusivity in the probe presheath zone ($D_{\perp ps}$), supporting the hypothesis that $\Gamma_{r\tilde{n}\tilde{\phi}} \sim \Gamma_{\perp probe}$.

However, the magnitude of $D'_{\perp ps}$ is clearly not directly tied to the magnitude of $D_{\perp SOL}$: $D_{\perp SOL}$ increases with discharge density to account for the increased particle flux across the profile (increased ionization rate) and the flatter density profiles (see Fig. 4); $D'_{\perp ps}$ is indifferent to this global particle balance requirement. But, in light of recent observations of large-scale 'bursty' transport in the far SOL of Alcator C-Mod[48,57,42], this inconsistency should not be entirely unexpected: Cross-field transport in the unperturbed SOL appears to involve transport events with spatial size-scale that is comparable to the width of the SOL. SOL transport physics may not be adequately described in terms of a single local parameter, $D_{\perp SOL}$. Moreover, assuming this physics also occurs in the probe's presheath zone, net particle flux into the probe's presheath region would involve smaller size-scale transport events.

$D'_{\perp ps}$ derived from both models appear to indicate a strong reduction in cross-field transport near the separatrix for the lowest plasma densities. It is interesting to note that for the highest density discharges, no reduction is seen; $D'_{\perp ps}$ is uniformly ~1 m^{-2} s^{-1} across the separatrix. This observation is consistent with the overall behavior of the SOL in Alcator C-Mod: As the density is raised, the distinct character of the fluctuations in the far SOL (i. e., bursty

transport behavior) starts to invade the closed flux surface regions. In the highest density discharges this bursty behavior is seen well inside the separatrix[48].

V. DISCUSSION

Interpreting $\Gamma_{r\tilde{n}\tilde{\phi}}$ as a measurement of the local particle fluxes in the unperturbed plasma in Alcator C-Mod clearly leads to some apparent inconsistencies with respect to global particle and energy balance. These problems mimic similar ones reported in other experiments, as outlined in the introduction. However, the problems can be resolved if one considers the perturbation that the probe body can have on these measurements: $\Gamma_{r\tilde{n}\tilde{\phi}}$ can be dominated by the plasma flux ($\Gamma_{\perp probe}$) that is needed to 'fill-in' the presheath plasma zone formed by the probe body. The data and analysis in this paper does indeed support the hypothesis that $\Gamma_{r\tilde{n}\tilde{\phi}} \sim \Gamma_{\perp probe}$, but only indirectly. A direct comparison of $D'_{\perp ps}$ with $D_{\perp ps}$ (or L' with L) could not be performed. Instead, values of $D'_{\perp ps}$ were compared with estimates of 'unperturbed' SOL values, $D_{\perp SOL}$.

It is important to know how to the properly interpret $\Gamma_{r\tilde{n}\tilde{\phi}}$ from probes since conclusions about plasma turbulence and the scaling of edge plasma conditions rely on these measurements. For example, in a study comparing turbulence data from TEXT, ATF, ZT-40M, Phaedrius-T and the Tokamak Fusion Test Reactor (TFTR) [58], it was found that the relationship,

$$\Gamma_{r\tilde{n}\tilde{\phi}} \approx 0.5 \frac{n C_s L_n}{L_c} \ , \qquad (19)$$

was approximately satisfied to within about a factor of ~2 over a range of $\Gamma_{r\tilde{n}\tilde{\phi}}$ that spanned over two orders of magnitude. Here L_n is the density gradient scale length and L_c is the characteristic connection length to the limiter in these devices. Based on this relationship, it was concluded that

one could simply infer $\Gamma_{r\tilde{n}\tilde{\phi}}$ from the right hand side of Eq. (19) in discharges where $\Gamma_{r\tilde{n}\tilde{\phi}}$ was not measured directly. Under the implicit assumption that $\Gamma_{r\tilde{n}\tilde{\phi}} \approx \Gamma_{\perp plasma}$, further conclusions about the scaling of $D_{\perp SOL}$ where then made. However, an alternative explanation for the observed relationship is that $\Gamma_{r\tilde{n}\tilde{\phi}} \approx \Gamma_{\perp probe}$. From the probe disk model [Eq. (9)],

$$\Gamma_{r\tilde{n}\tilde{\phi}} \approx \Gamma_{\perp probe} \approx 0.5 \frac{n C_s a}{2L}, \qquad (20)$$

which leads to the observed scaling relationship when $a/L \sim L_n / L_c$, a condition that is satisfied when $D_{\perp ps} \sim D_{\perp SOL}$. Although in this instance the conclusions that were made about $D_{\perp SOL}$ may not change, the interpretation, $\Gamma_{r\tilde{n}\tilde{\phi}} \approx \Gamma_{\perp probe}$, is fundamentally different and could be extremely important in other circumstances: Had the probe been inserted into a region of plasma where $\Gamma_{\perp plasma} \approx 0$ in these experiments (perhaps well inside the limiter radius), then the probe would still report a large value of $\Gamma_{r\tilde{n}\tilde{\phi}}$ ($\approx \Gamma_{\perp probe}$).

Recently, cross-field profiles of $\Gamma_{r\tilde{n}\tilde{\phi}}$ were measured during discharges in Alcator C-Mod which exhibited a quasi-coherent fluctuation, localized to a 1-2 mm region near the separatrix[59]. The magnitude of $\Gamma_{r\tilde{n}\tilde{\phi}}$ was found to peak very sharply in the vicinity of the mode layer, having values a factor of ~5 or more higher than on either side of the layer. Although an enhanced particle flux supported the overall observation that particle losses through the separatrix were higher in these discharges, the shape and magnitude of the flux profile was a puzzle: How could this rapidly varying radial flux profile satisfy the particle continuity equation across the separatrix and into the SOL? Also, the large convected power implied by the particle flux was difficult to reconcile. However, the interpretation, $\Gamma_{r\tilde{n}\tilde{\phi}} \approx \Gamma_{\perp probe}$, offers an obvious explanation: When the probe is inserted into the mode layer, particles are efficiently transported onto the probe body; this transport

rate is not simply related to the transport rate in the unperturbed plasma.

One could imagine designing an experiment to directly determine conditions under which the fluctuation-induced flux is a true measure of the transport flux in the unperturbed plasma. A simple test might be to design a probe such as the 'disk probe' shown in Fig. 8b, but with sets of electrodes spaced around the circumference of the disk. A strong gradient in plasma conditions would be in the radial direction, while, ideally, the mechanical support for the probe would be orthogonal to this gradient in the vicinity of the probe. If it is found that the flux at all points around the circumference of the probe disk are directed toward the probe's shadow, then the hypothesis, $\Gamma_{r\tilde{n}\tilde{\phi}} \sim \Gamma_{\perp probe}$, would be explicitly proved. In that case, a probe such as that shown in Fig. 1 would not be able to measure the transport fluxes in the unperturbed plasma.

VI. SUMMARY AND CONCLUSIONS

The reliability of an electrostatic probe to deduce the fluctuation-induced particle fluxes in the unperturbed plasma has been critically assessed for a series of discharges in Alcator C-Mod. Comparisons of the measured fluxes with those from global particle and energy balance show clear inconsistencies in magnitude and profile shape which can not be simply resolved. These observations suggest that the fluctuation-induced particle flux estimates made by the C-Mod probe should not be interpreted as indicative of the transport in the unperturbed plasma. Similar inconsistencies have been reported in other experiments. However, if the fluctuation-induced flux is reinterpreted as a measure of the local flux into the probe's presheath region, the inconsistencies can be resolved. In this case, an effective cross-field diffusivity in the probe's presheath zone can be estimated from the fluctuation-induced flux measurement. Its magnitude is found to be in the range of diffusivities in the unperturbed plasma, indirectly supporting the new interpretation. However, it is not clear how this effective presheath diffusivity is related to the transport in the unperturbed plasma; its profile shape and scaling with discharge conditions does not track the effective diffusivities found from global particle balance. A simple experiment is suggested which might help

identify the conditions (if any) under which the fluctuation-induced particle fluxes from an electrostatic probe can be related to the transport rate in the unperturbed plasma.

Acknowledgements

The data presented in this paper would not have been collected without the continuing dedication and hard work of the engineers, technical staff, students, and scientists on the Alcator team. The author thanks Ben Carreras for encouragement to work in the area of fluctuations and turbulent transport, Martin Greenwald for setting up the high density plasmas, Ian Hutchinson and Stewart Zweben for valuable comments and the entire C-Mod physics staff for scheduling and running these ohmic L-mode discharges. This work is supported by U.S. D.o.E. Coop. Agreement DE-FC02-99ER54512.

REFERENCES

[1]J. A. Wesson, Plasma Physics and Controlled Fusion **37**, 1459 (1995).

[2]O. V. Batishchev, S. I. Krasheninnikov, P. J. Catto *et al.*, Physics of Plasmas **4**, 1672 (1997).

[3]J. G. Watkins, O. Batishchev, J. Boedo *et al.*, Journal of Nuclear Materials **266**, 980 (1999).

[4]R. A. Pitts, Bull. Am. Phys. Soc. **45** (2000).

[5]P. C. Stangeby, Journal of Nuclear Materials **121**, 36 (1984).

[6]I. H. Hutchinson, Physical Review a **37**, 4358 (1988).

[7]I. H. Hutchinson, Physics of Fluids B Plasma Physics **3**, 847 (1991).

[8]G. F. Matthews, P. C. Stangeby, and P. Sewell, Journal of Nuclear Materials **145-147**, 220 (1987).

[9]K. S. Chung, I. H. Hutchinson, B. LaBombard, and R. W. Conn, Physics of Fluids B Plasma Physics **1**, 2229 (1989).

[10]G. F. Matthews and P. C. Stangeby, J. Phys. D. **22**, 644 (1989).

[11]S. Zweben, P. C. Liewer, and R. W. Gould, Journal of Nuclear Materials **111**, 39 (1982).

[12]S. J. Levinson, J. M. Beall, E. J. Powers, and R. D. Bengtson, Nuclear Fusion **24**, 527 (1984).

[13]C. P. Ritz, R. V. Bravenec, R. D. Bengtson *et al.*, Journal of Nuclear Materials **145**, 241 (1987).

[14]Yang Shikun, Yang Qingwei, Ding Xuantong *et al.*, Journal of Nuclear Materials **176**, 699 (1990).

[15]A. J. Wootton, Journal of Nuclear Materials **176**, 77 (1990).

[16]T. Uckan, C. Hidalgo, J. D. Bell *et al.*, Physics of Fluids B (Plasma Physics) **3**, 1000 (1991).

[17]R. A. Moyer, J. G. Watkins, R. W. Conn *et al.*, Journal of Nuclear Materials **196**, 854 (1992).

[18]H. Y. W. Tsui, D. M. Manos, A. Rudyj, C. P. Ritz, and A. J. Wootton, Journal of Nuclear Materials **196**, 292 (1992).

[19]G. R. Tynan, L. Schmitz, L. Blush *et al.*, Physics of Plasmas **1**, 3301 (1994).

[20]M. Endler, H. Niedermeyer, L. Giannone, E. Kolzhauer, A. Rudyj, G. Theimer, and N. Tsois, Nuclear Fusion **35**, 1307 (1995).

[21]B. A. Carreras, C. Hidalgo, E. Sanchez *et al.*, Physics of Plasmas **3**, 2664 (1996).

[22]I. Garcia Cortes, C. Hidalgo, J. R. Martin Solis *et al.*, Plasma Physics and Controlled Fusion **38**, 2051 (1996).

[23]R. A. Moyer, J. W. Cuthbertson, T. E. Evans, G. D. Porter, and J. G. Watkins, Journal of Nuclear Materials **241**, 633 (1997).

[24]M. Endler, Journal of Nuclear Materials **266**, 84 (1999).

[25]C. Hidalgo, C. Silva, M. A. Pedrosa, E. Sanchez, H. Fernandes, and C. A. F. Varandas, Physical Review Letters **83**, 2203 (1999).

[26]I. Garcia Cortes, A. Loarte, R. Balbin *et al.*, Journal of Nuclear Materials **290**, 604 (2001).

[27]P. Ritz Ch, R. V. Bravenec, P. M. Schoch *et al.*, Physical Review Letters **62**, 1844 (1989).

[28]G. R. Tynan, R. A. Moyer, M. J. Burin, and C. Holland, Physics of Plasmas **8**, 2691 (2001).

[29]E. Sanchez, C. Hidalgo, D. Lopez Bruna *et al.*, Physics of Plasmas **7**, 1408 (2000).

[30]J. A. Boedo, D. Rudakov, R. Moyer *et al.*, Physics of Plasmas **8**, 4826 (2001).

[31]S. J. Zweben and R. W. Gould, Nuclear Fusion **25**, 171 (1985).

[32]W. L. Rowan, C. C. Klepper, C. P. Ritz *et al.*, Nuclear Fusion **27**, 1105 (1987).

[33]S. J. Zweben, J. McChesney, and R. W. Gould, Nuclear Fusion **23**, 825 (1983).

[34]C. Alejaldre, J. Alonso, L. Almoguera *et al.*, Plasma Physics and Controlled Fusion **41**, A539 (1999).

[35]L. Garcia, B. A. Carreras, V. E. Lynch, M. A. Pedrosa, and C. Hidalgo, Physics of Plasmas **8**, 4111 (2001).

[36]G. F. Matthews, G. Corrigan, S. K. Erents *et al.*, to be published in Plasma Physics and Controlled Fusion.

[37]V. P. Budaev, L. M. Bogomolov, B. V. Borovsky *et al.*, Journal of Nuclear Materials **176**, 705 (1990).

[38]R. A. Moyer, R. Van Nieuwenhove, G. Van Oost *et al.*, Journal of Nuclear Materials **176**, 293 (1990).

[39]G. R. Tynan, L. Schmitz, R. W. Conn, R. Doerner, and R. Lehmer, Physical Review Letters **68**, 3032 (1992).

[40]M. J. Schaffer, B. D. Bray, J. A. Boedo *et al.*, Physics of Plasmas **8**, 2118 (2001).

[41]M. A. Meier, R. D. Bengtson, G. A. Hallock, and A. J. Wootton, Physical Review Letters **87**, 085003 (2001).

[42]S. Zweben, Bull. Am. Phys. Soc. **46** (2001).

[43]I. H. Hutchinson, R. Boivin, F. Bombarda *et al.*, Physics of Plasmas **1**, 1511 (1994).

[44]B. LaBombard, S. Gangadhara, B. Lipschultz *et al.*, Elsevier. Journal of Nuclear Materials **266-269**, 571 (1999).

[45]R. L. Boivin, J. A. Goetz, A. E. Hubbard *et al.*, Physics of Plasmas **7**, 1919 (2000).

[46]B. LaBombard, M. V. Umansky, R. L. Boivin *et al.*, Nuclear Fusion **40**, 2041 (2000).

[47]L. C. Johnson and E. Hinnov, Journal of Quantitative Spectroscopy & Radiative Transfer **13**, 333 (1973).

[48]B. LaBombard, R. L. Boivin, M. Greenwald *et al.*, Physics of Plasmas **8**, 2107 (2001).

[49]P. C. Stangeby, Physics of Fluids **27**, 682 (1984).

[50]J. M. Beall, Y. C. Kim, and E. J. Powers, Journal of Applied Physics **53**, 3933 (1982).

[51]R. A. Langley, J. Bohdansky, W. Eckstein *et al.*, eds. *Data compendium for plasma-surface interactions*. Nuclear Fusion, Special Issue, IAEA, Vienna (1984).

[52]R. K. Janev, *Elementary processes in hydrogen-helium plasmas : cross sections and reaction rate coefficients* (Springer-Verlag, Berlin ; New York, 1987).

[53]P. C. Stangeby, Physics of Fluids **27**, 2699 (1984).

[54]I. H. Hutchinson, Physics of Fluids **30**, 3777 (1987).

[55]M. V. Umansky, S. I. Krasheninnikov, B. LaBombard, and J. L. Terry, Physics of Plasmas **5**, 3373 (1998).

[56]M. V. Umansky, S. I. Krasheninnikov, B. LaBombard, B. Lipschultz, and J. L. Terry, Physics of Plasmas **6**, 2791 (1999).

[57]J. L. Terry, R. Maqueda, C. S. Pitcher *et al.*, Journal of Nuclear Materials **290**, 757 (2001).

[58]H. Y. W. Tsui, A. J. Wootton, J. D. Bell *et al.*, Journal of Nuclear Materials **196**, 794 (1992).

[59]A. E. Hubbard, R. L. Boivin, R. S. Granetz *et al.*, Physics of Plasmas **8**, 2033 (2001).

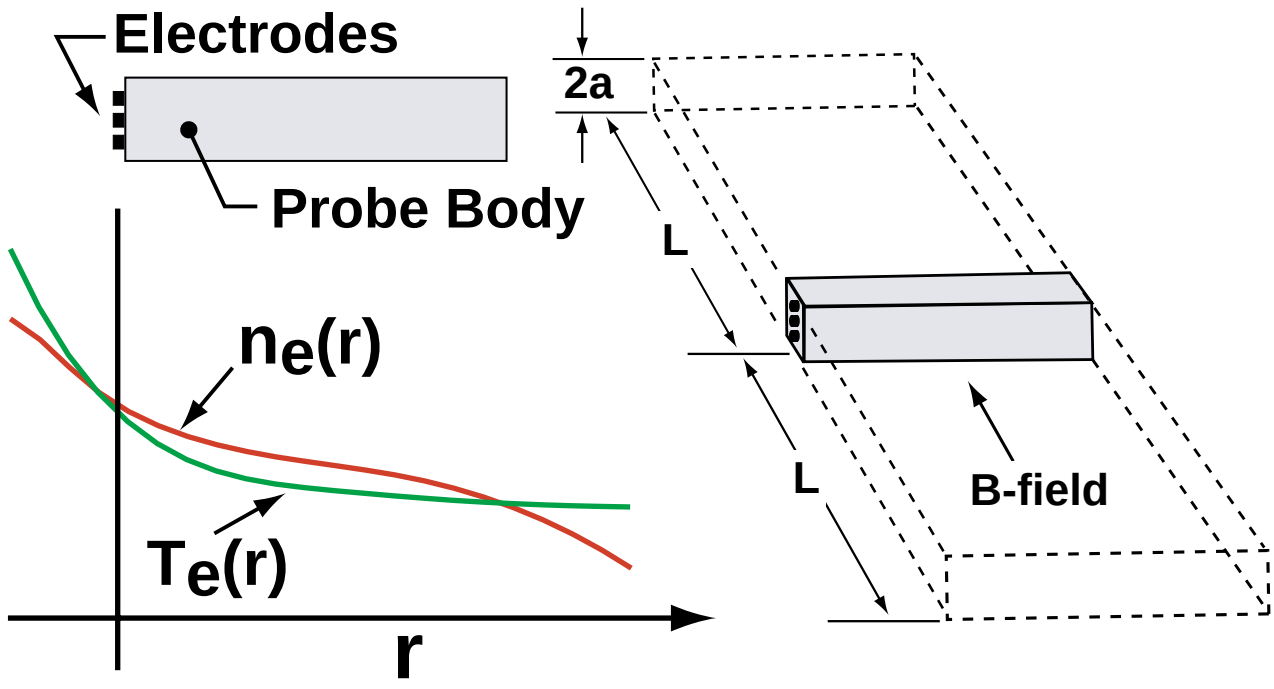

Fig. 1. A turbulence transport probe usually employs set of electrodes protruding from the end of a probe body. Such a probe is typically inserted into a scrape-off layer with strong cross-field variation in density (n) and temperature (T). The probe body induces a density-depressed (pre-sheath) plasma zone, extending along magnetic field lines over a characteristic distance (L). Cross-field plasma flow into the pre-sheath zone balances parallel plasma flow onto the probe body.

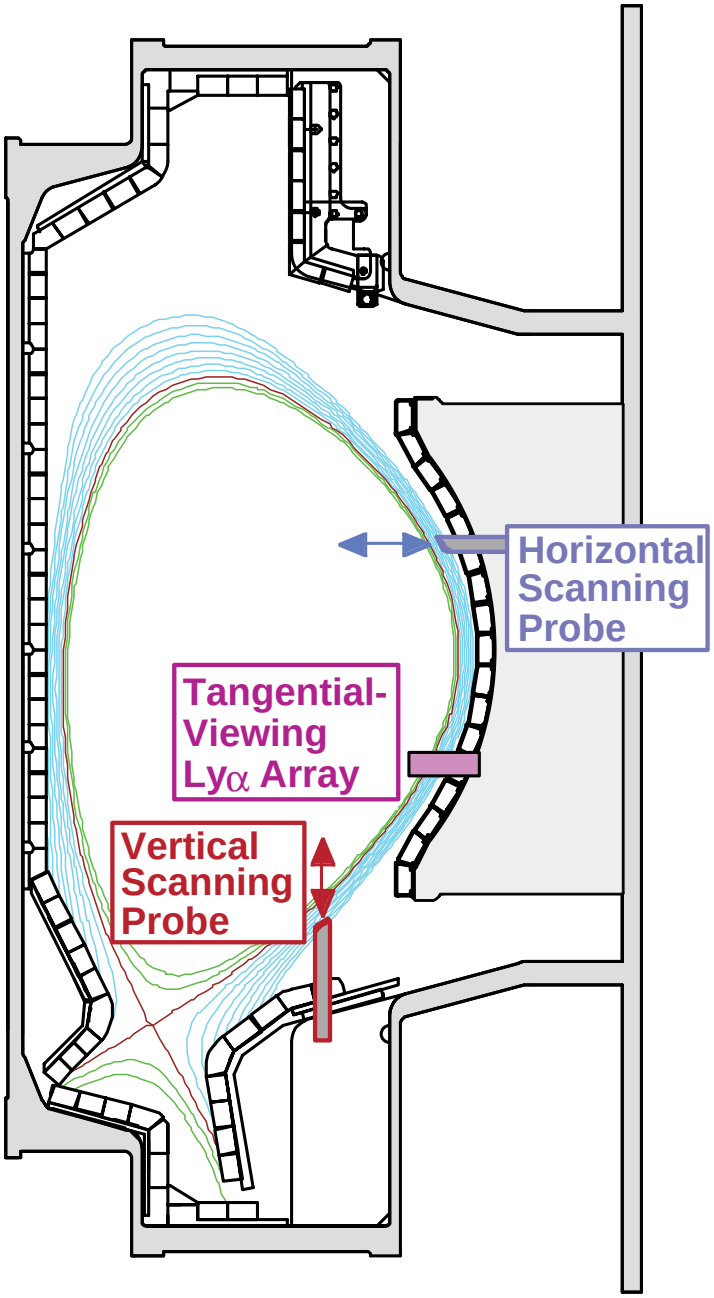

Fig. 2. Cross-section of Alcator C-Mod showing locations of diagnostics and a plasma equilibrium used for these studies. In addition to recording time-averaged density and temperature profiles, the horizontal probe is used to record fluctuation-induced particle fluxes. Cross-field fluxes are separately estimated from scrape-off layer particle balance, with the aid of plasma flow measurements from the vertical probe and ionization profile estimates from the toroidally-viewing Lyα diagnostic[45].

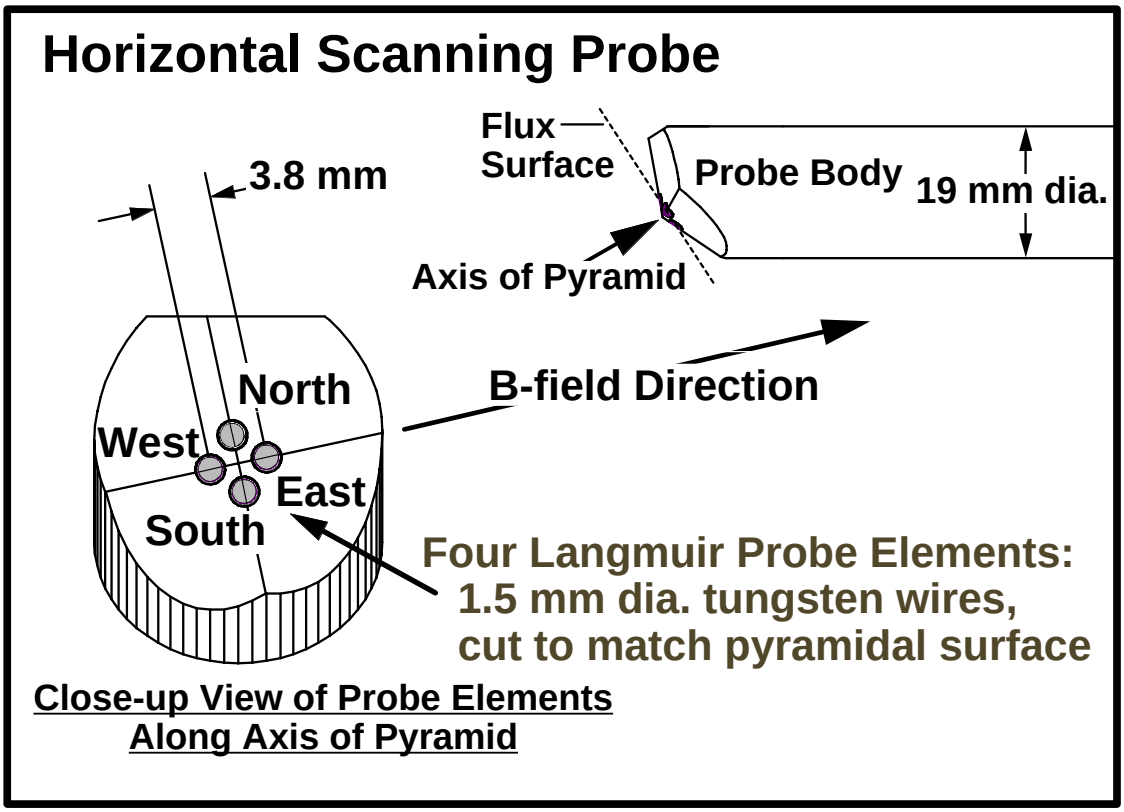

Fig. 3. Close-up view of electrode geometry for the horizontal scanning probe. Four electrodes are equally spaced around the apex of a pyramid and machined to match its surfaces. The NORTH and SOUTH probes record voltage fluctuations while the EAST and WEST probes record ion current fluctuations.

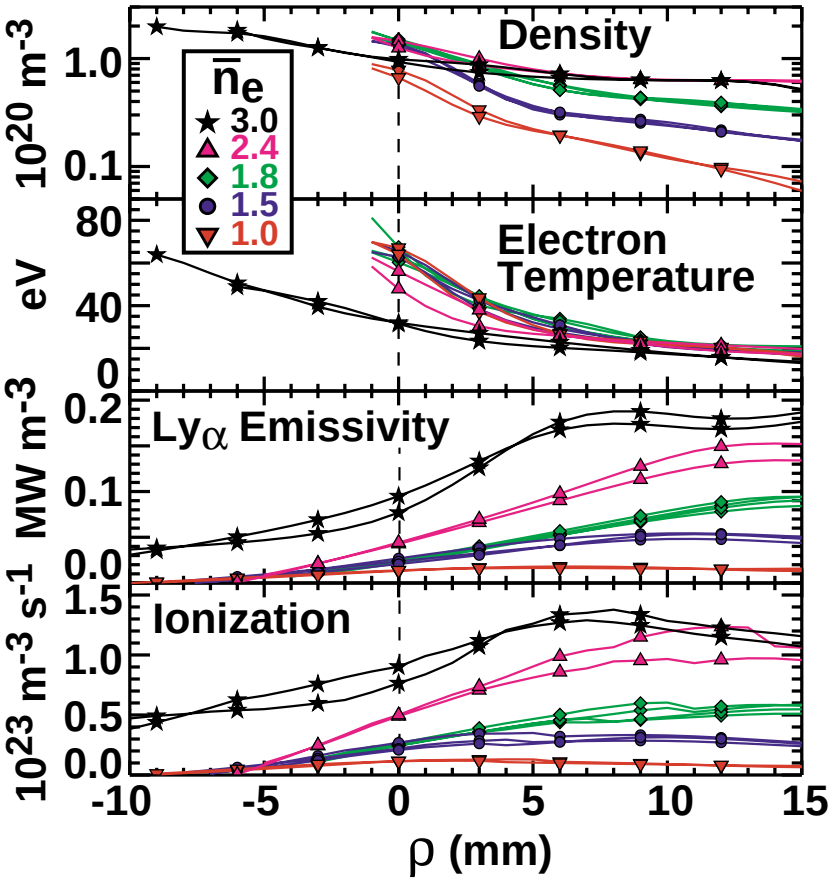

Fig. 4. Cross-field profiles for a range of line-averaged plasma densities ($\bar{n}_e$). Two or more profiles are shown for each density case. Top two panels: Density and electron temperature from horizontal scanning probe (smooth spline fit to data points). Third panel: Lyα emissivity from Abel inversion of spline-fitted brightness data. Last panel: Ionization source strength inferred from data in other panels. All data are plotted versus distance into the scrape-off layer, mapped to the outer midplane.

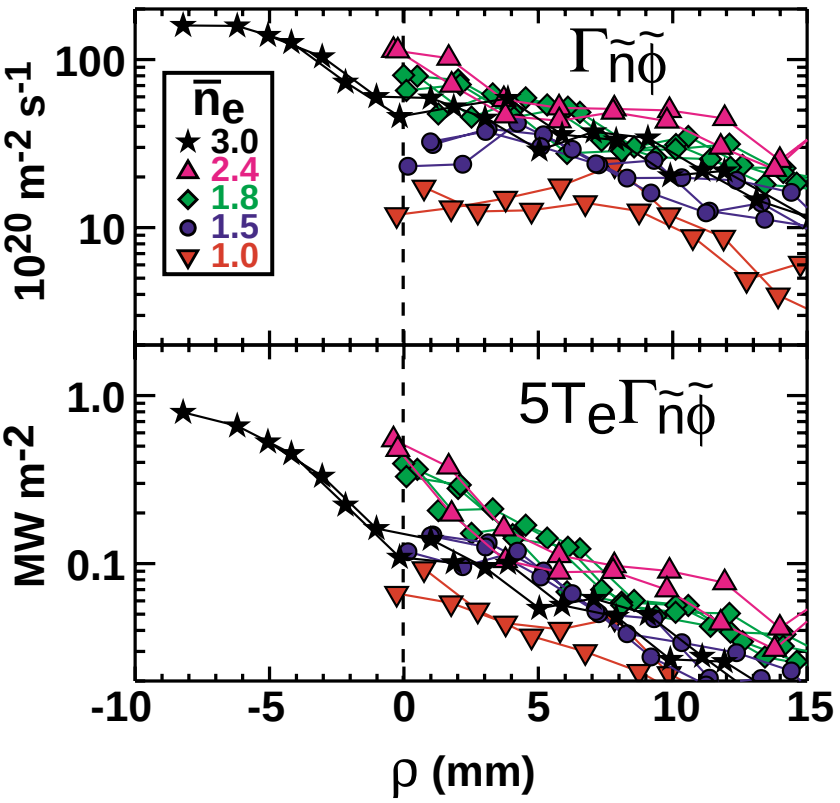

Fig. 5. Cross-field profiles of measured fluctuation-induced particle flux density (top panel) and implied heat convection (bottom panel) corresponding to the discharges represented in Fig. 4. Profiles deep inside the separatrix are obtained only in the highest density discharge. Particle flux densities continue to increase inside the separatrix in apparent contradiction to global particle balance.

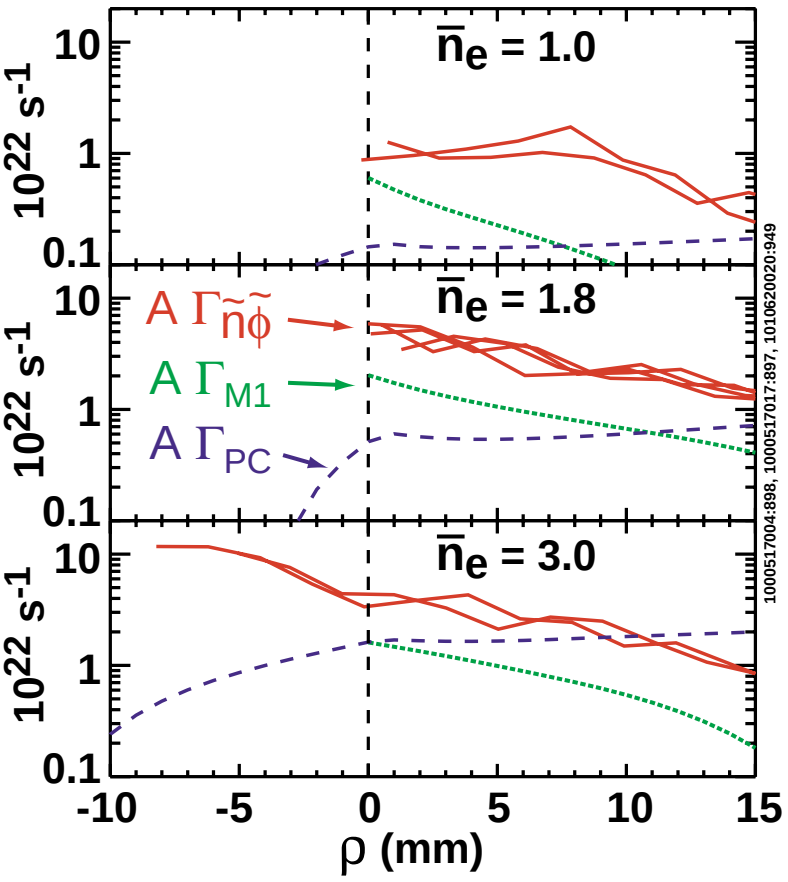

Fig. 6. Comparisons of total cross-field particle fluxes: fluctuation-induced particle flux measurement (solid), flux from Mach 1 flow model (dotted), flux from SOL particle continuity model (dashed). Each panel corresponds to a different discharge density. For clarity, curves from only a single discharge is shown for the latter two parameters in each panel. Both the magnitudes and shapes of the fluctuation-induced particle flux profiles are not easily reconciled with global particle balance considerations.

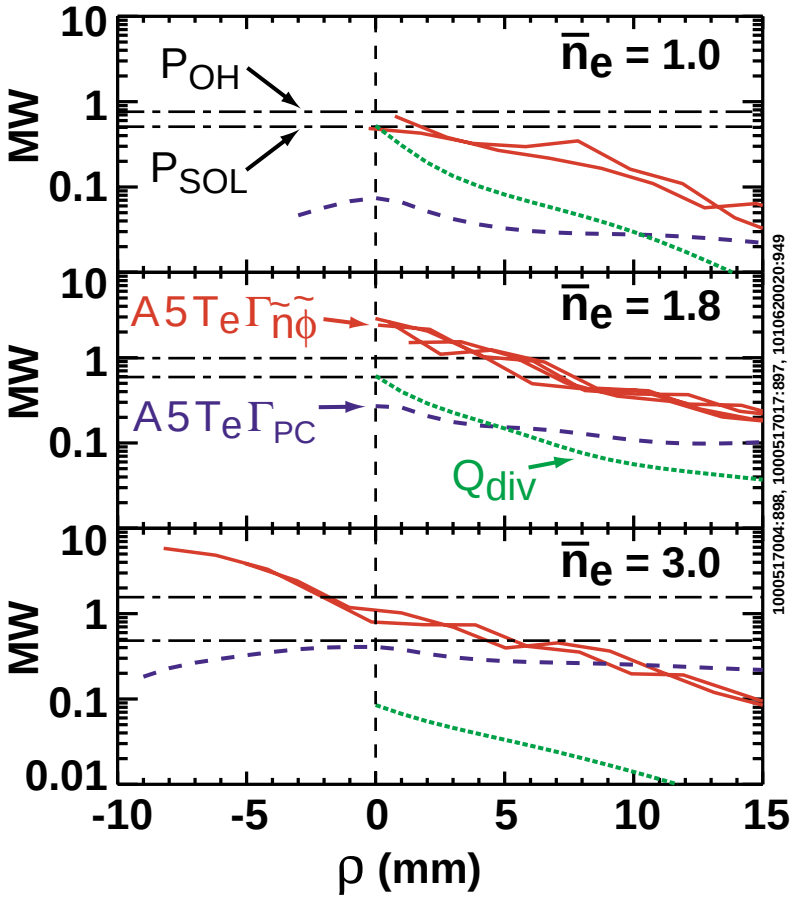

Fig. 7. Comparisons of total heat flux crossing magnetic flux surfaces: heat convection from fluctuation-induced particle flux measurement (solid), same quantity from SOL particle continuity model (dashed), heat necessary to support electron conduction losses to the divertor (dotted). Each panel corresponds to a different discharge density. For clarity, curves from only a single discharge are shown for the latter two parameters in each panel. The horizontal lines (dash-dot) correspond to total input power and the power into the SOL in these discharges. The fluctuation-induced fluxes lead to obvious inconsistencies in magnitude and shape relative to global power balance constraints.

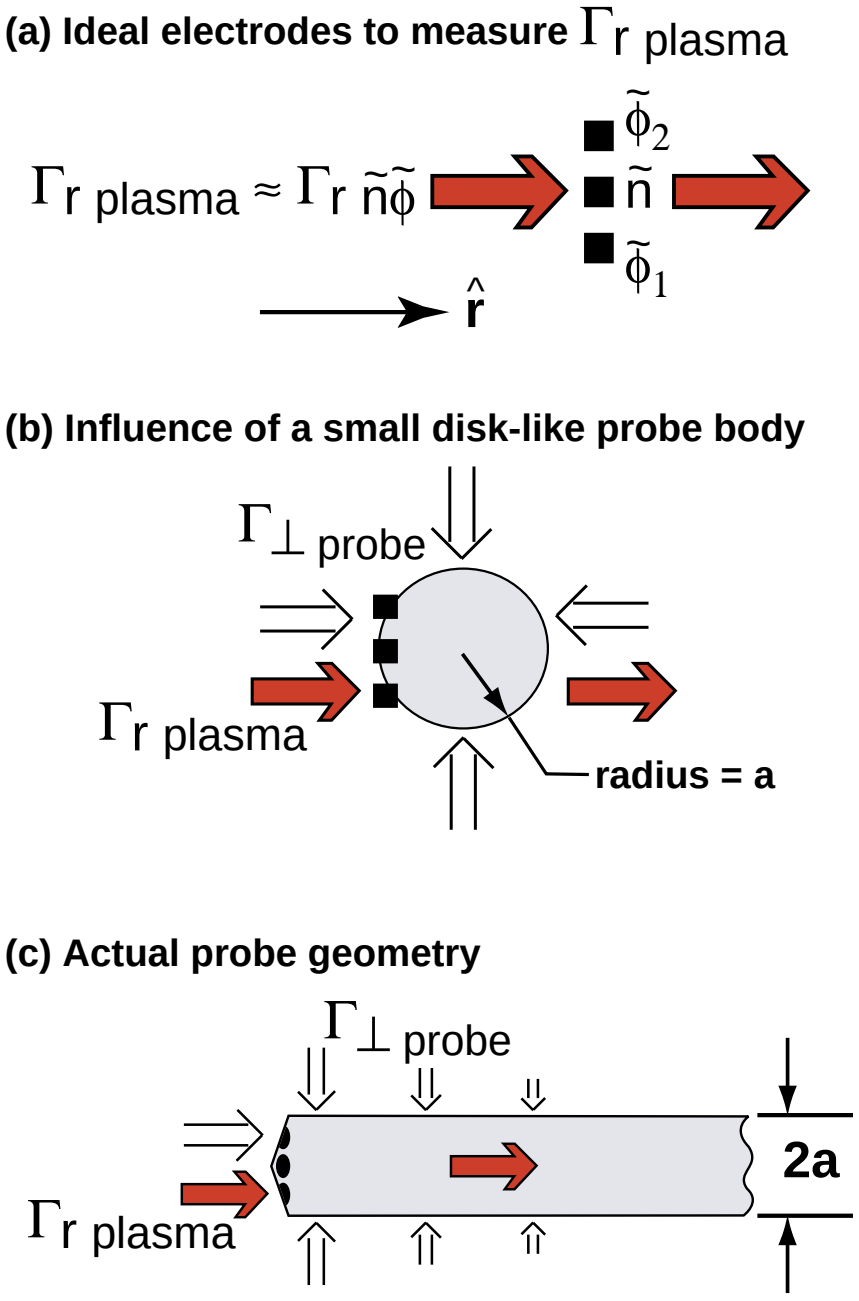

Fig. 8. Ideal turbulence probe geometry (a) and practical turbulence probe geometries (b and c). In order to electrically connect and mechanically support three electrodes for a turbulence-induced flux estimate, a probe body structure is required. A small 'disk probe' lends itself to a simple transport analysis. The actual probe geometry is more complex, with significant variation in plasma parameters across the probe body.

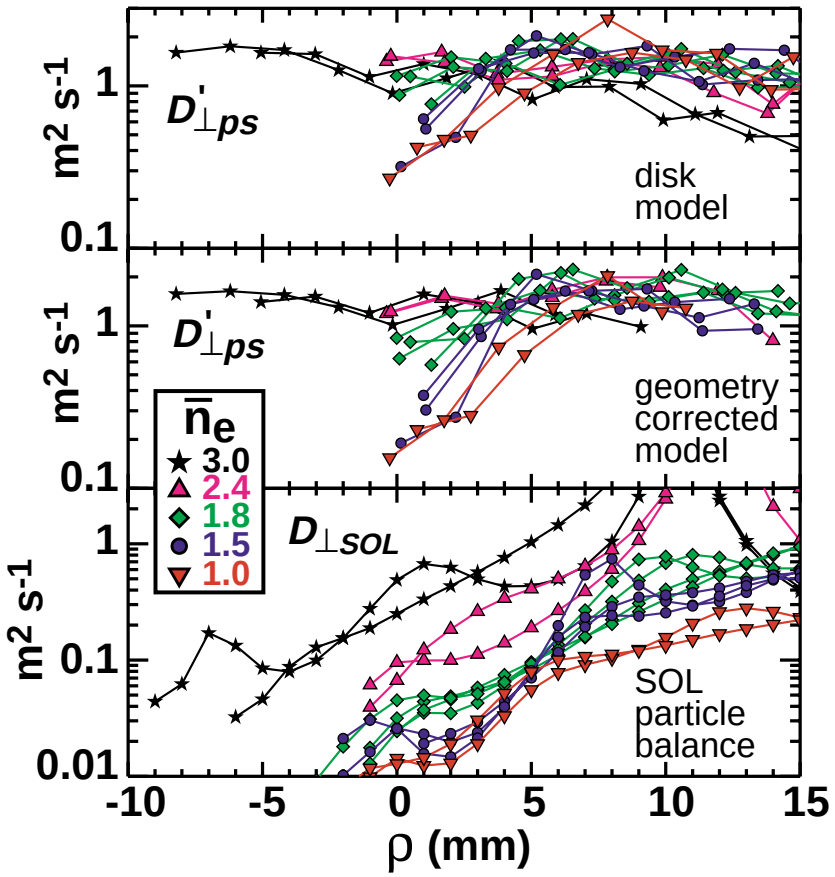

Fig. 9. Comparison of three effective cross-field particle diffusivity profiles: presheath diffusivity from 'probe disk' model (top), presheath diffusivity from geometry-corrected model (middle), and the unperturbed SOL diffusivity from SOL particle continuity model (note different vertical scale). Profiles are obtained from the same set of discharges shown in Fig. 4. Both presheath diffusivities have roughly fixed levels in the far SOL with a trend of decreasing values as the separatrix is approached, depending on the density of the discharge. In comparison, the unperturbed SOL diffusivity profile has more of a fixed shape, with its overall magnitude changing with discharge density. Thus the presheath diffusivities do not appear to be directly related to effective diffusivities in the unperturbed SOL.